Decomposition of Methanthiol on Pt(111): A Density Functional Investigation

ARTICLE *in* LANGMUIR · JULY 2010

Impact Factor: 4.46 · DOI: 10.1021/la101678d · Source: PubMed

8 AUTHORS, INCLUDING:

Houyu Zhu
University of Notre Dame
35 PUBLICATIONS **661** CITATIONS
SEE PROFILE

Ruibin Jiang
The Chinese University of Hong Kong
29 PUBLICATIONS **778** CITATIONS
SEE PROFILE

Langmuir
Article
pubs.acs.org/Langmuir

Decomposition of Methanthiol on Pt(111): A Density Functional Investigation

Houyu Zhu,[†] Wenyue Guo,*[,†] Ruibin Jiang,[†] Lianming Zhao,[†] Xiaoqing Lu,[§] Ming Li,[†] Dianling Fu,[†] and Honghong Shan*[,‡]

[†]*College of Physics Science and Technology, and* [‡]*State Key Laboratory for Heavy Oil Processing, China University of Petroleum Dongying, Shandong 257061, PR China, and* [§]*Department of Physics and Materials Science, City University of Hong Kong, Hong Kong SAR, People's Republic of China*

Received April 26, 2010. Revised Manuscript Received June 9, 2010

Decomposition of methanthiol on Pt(111) is systematically investigated using self-consistent periodic density functional theory (DFT), and the decomposition network has been mapped out. The most stable adsorption of the involved species tends to form the sp^3 hybridized configuration of both C and S atoms, in which C is almost tetrahedral and S has the tendency to bond to three atoms. Spontaneous dissociation rather than desorption is preferred for adsorbed methanthiol. Based on the harmonic transition state theory calculations, the decomposition rate constants of the thiolmethoxy and thioformaldehyde intermediates are found to be much lower than those for their formation, leading to long lifetimes of the intermediates for observation. Under the ultrahigh vacuum (UHV) condition, the most possible decomposition pathway for methanthiol on Pt(111) is found as $CH_3SH \rightarrow CH_3S \rightarrow CH_2S \rightarrow CHS \rightarrow CH + S \rightarrow C + S$, in which the C−S bond cleavage mainly occurs at the CHS species. However, the decomposition pathway is $CH_3SH \rightarrow CH_3S \rightarrow CH_3 + S$ under the hydrogenation condition; the C−S bond scission mainly occurs at CH_3S. The Brønsted−Evans−Polanyi relation holds for each of the S−H, C−H, and C−S bond scission reactions.

1. Introduction

The catalytic desulfurization of sulfur-containing hydrocarbons has attracted widespread attention because small amounts of sulfur in gasolines and gasoil fuels are increasingly in demand to meet the global environmental regulations.[1,2] In the petroleum industry, hydrodesulfurization (HDS) is one of the most important processes to produce clean fuels, in which CoMo and NiMo sulfides are widely used as conventional HDS catalysts.[3] Recently, the development of highly active HDS catalysts (e.g., supported noble metal catalysts,[4−6] which are more active than the commercial CoMo and NiMo materials) has been claimed in the petroleum industry to produce fuels with much low sulfur contents. The key step of the desulfurization process is the C−S bond cleavage, which is still not well understood. The poor performance of surface spectroscopic techniques toward metal sulfides hinders progress in understanding the mechanism of the C−S bond cleavage on metal sulfide surfaces. However, pure metal surfaces can be readily characterized by spectroscopic techniques, making them ideal for surface science model studies.

Owing to their relatively simple structures, much work has been done on the interaction of thiols (R−SH) with metal surfaces to explore more options of highly active catalysts for HDS.[7−22] As the simplest thiol, methanethiol is often used as a model molecule in surface science studies because it lacks the β-carbon atom and thus is perfectly suitable for studying the S−H bond activation and, more importantly, the catalytic C−S bond scission. In order to clarify the catalytic performance of different metals, decomposition of methanethiol has been investigated using various surface science techniques on various pure metal surfaces, including W(211),[7] Cu(100),[9] Fe(100),[10] Mo(110),[13] W(001),[16] Ni(111),[11,17] Ni(100),[15] Fe(110),[19] Ni(110),[20] Pt(111),[8,12,14,18,21] and Au(111).[22] Also, adsorption and S−H bond scission of methanethiol on Au(111) and Pd(111) have been studied using periodic, self-consistent density functional theory (DFT) calculations.[23−25] These investigations have demonstrated that the low-temperature surface chemistry of methanethiol strongly depends on the identity of the metals.

*To whom correspondence should be addressed. E-mail: wyguo@upc.edu.cn (W.G.); shanhh@upc.edu.cn (H.S.) Telephone: 86-546-839-6634. Fax: 86-546-839-7511.

(1) Friend, C. M.; Chen, D. A. *Polyhedron* **1997**, *16*, 3165.
(2) Weigand, B. C.; Friend, C. M. *Chem. Rev.* **1992**, *92*, 491.
(3) Topsøe, H.; Clausen, B. S.; Massoth, F. E. *Hydrotreating Catalysis, Science and Technology*; Springer: Berlin, 1996.
(4) Sugioka, M.; Sado, F.; Kurosaka, T.; Wang, X. *Catal. Today* **1998**, *45*, 327.
(5) Sugioka, M.; Andalaluna, L.; Morishita, S.; Kurosaka, T. *Catal. Today* **1997**, *39*, 61.
(6) Sun, Y. Y.; Wang, H. M.; Prins, R. *Catal. Today* **2010**, *150*, 213.
(7) Benziger, J. B.; Preston, R. E. *J. Phys. Chem.* **1985**, *89*, 5002.
(8) Koestner, R. J.; Stöhr, J.; Gland, J. L.; Kollin, E. B.; Sette, F. *Chem. Phys. Lett.* **1985**, *120*, 285.
(9) Sexton, B. A.; Nyberg, G. L. *Surf. Sci.* **1986**, *165*, 251.
(10) Albert, M. R.; Lu, J. P.; Bernasek, S. L.; Cameron, S. D.; Gland, J. L. *Surf. Sci.* **1988**, *206*, 348.
(11) Castro, M. E.; White, J. M. *Surf. Sci.* **1991**, *257*, 22.
(12) Rufael, T. S.; Prasad, J.; Fischer, D. A.; Gland, J. L. *Surf. Sci.* **1992**, *278*, 41.
(13) Wiegand, B. C.; Uvdal, P.; Friend, C. M. *Surf. Sci.* **1992**, *279*, 105.
(14) Rufael, T. S.; Koestner, R. J.; Kollin, E. B.; Salmeron, M.; Gland, J. L. *Surf. Sci.* **1993**, *297*, 272.
(15) Parker, B.; Gellman, A. J. *Surf. Sci.* **1993**, *292*, 223.
(16) Mullins, D. R.; Lyman, P. F. *J. Phys. Chem.* **1993**, *97*, 9226.
(17) Rufael, T. S.; Huntley, D. R.; Mullins, D. R.; Gland, J. L. *J. Phys. Chem.* **1995**, *99*, 11472.
(18) Kim, S. S.; Kim, Y.; Kim, H. I.; Lee, S. H.; Lee, T. R.; Perry, S. S.; Rabalais, J. W. *J. Chem. Phys.* **1998**, *109*, 9574.
(19) Batteas, J. D.; Rufael, T. S.; Friend, C. M. *Langmuir* **1999**, *15*, 2391.
(20) Huntley, D. R. *J. Phys. Chem.* **2002**, *93*, 6156.
(21) Lin, T. H.; Huang, T. P.; Liu, Y. L.; Yeh, C. C.; Lai, Y. H.; Hung, W. H. *Surf. Sci.* **2005**, *578*, 27.
(22) Maksymovych, P.; Sorescu, D.; Yates, J. *J. Phys. Chem. B* **2006**, *110*, 21161.
(23) Gottschalck, J.; Hammer, B. *J. Chem. Phys.* **2002**, *116*, 784.
(24) Majumder, C. *Langmuir* **2008**, *24*, 10838.
(25) Lustemberg, P. G.; Martiarena, M. L.; Martinez, A. E.; Busnengo, H. F. *Langmuir* **2008**, *24*, 3274.

Platinum is an effective catalyst for many petrochemical processes.[26] When supported on zeolites[4] and related materials (such as mesoporous silicate),[5] platinum exhibits high activity for the HDS of organic sulfur compounds, making it a potential second-generation catalyst for deep HDS. The Pt(111) surface is often considered because it is the most stable Pt surface that dominates in small particles used in catalysts. On Pt(111), under the ultrahigh vacuum (UHV) condition, high-resolution electron energy loss spectroscopy (HREELS), temperature programmed desorption (TPD), and near-edge X-ray absorption fine structure spectroscopy (NEXAFS) experiments have determined the structure and orientation of the methylthiolate and methylenesulfide intermediates formed during thermal decomposition of adsorbed methanethiol.[8,14] Further studies, combined with low-energy electron diffraction (LEED) and X-ray photoelectron spectroscopy (XPS) techniques, indicated that sequential dehydrogenation occurs until S and C atoms are formed.[18,21] However, under hydrogenation conditions, Rufael et al. found that CH_4 is the primary product for the decomposition of methanethiol at around 300 K via TPD combined with in situ fluorescence yield near edge spectroscopy (FYNES), indicating that the reaction involving the C−S bond scission may prevail.[12]

In spite of these experimental works, to our knowledge, no theoretical reports are available to illustrate the complete mechanism of thiol adsorption and decomposition, especially the C−S bond scission, on Pt surfaces. Furthermore, the decomposition pathways of methanthiol on Pt(111) under different (UHV and hydrogenation) conditions revealed by experiments[8,14,18,21] should been clarified. These facts motivate us to proceed a theoretical investigation of methanthiol decomposition on Pt(111) based on the periodic, self-consistent DFT calculations. In this paper, we consider the most possible pathways involving the C−H, S−H, and C−S bond scission for methanthiol decomposition. We address both the structures and energies of the involved intermediates and present the detailed potential energy surfaces (PES). Also, we discuss the decomposition mechanism of methanthiol based on kinetic analysis.

2. Computational Details

The DFT calculations were performed with the program package of DMol[3] in Materials Studio of Accelrys Inc.[27−29] The exchange-correlation energy was calculated within the generalized gradient approximation (GGA) using the form of the functional proposed by Perdew and Wang,[30,31] usually referred to as Perdew−Wang 91 (PW91). To take the relativity effect into account, the density functional semicore pseudopotential (DSPP) method was employed for the Pt atoms, and the carbon, sulfur, and hydrogen atoms were treated with an all-electron basis set. The valence electron functions were expanded into a set of numerical atomic orbitals by a double-numerical basis with polarization functions (DNP). A Fermi smearing of 0.005 hartree and a real-space cutoff of 4.5 Å were used to improve the computational performance. All computations were performed with spin-polarization.

The lattice constant of the bulk platinum was calculated to be 4.006 Å, in good agreement with the experimental value (3.912 Å).[32] This calculated lattice constant was subsequently used in all calculations to maintain a true energy minimum with respect to the bulk Pt reference state. The Pt(111) surface was modeled by a four-layer slab with four platinum atoms per layer representing a $p(2 \times 2)$ unit cell, and a vacuum region of 16 Å thickness was used to separate the surface from its periodic image in the direction along the surface normal. The reciprocal space was sampled by a grid of $(5 \times 5 \times 1)$ k-points generated automatically using the Monkhorst−Pack method.[33] A single adsorbate was allowed to adsorb on one side of the (2×2) unit cell, corresponding to a surface coverage of 25%. Full-geometry optimization was performed for all relevant adsorbates and the uppermost two layers without symmetry restriction, while the bottom two layer Pt atoms were fixed at the positions at the calculated lattice constant. The tolerances of energy, gradient, and displacement convergence were 1×10^{-5} hartree, 2×10^{-3} hartree/Å, and 5×10^{-3} Å, respectively. At the present theoretical level, the average S−Pt bond length for an adsorbed S atom at a fcc site was calculated to be 2.303 Å, agreeing well with the LEED result of 2.28 ± 0.03 Å.[34]

Nonperiodical structures were fully optimized at the same theoretical level for the isolated atoms, radicals, and molecules involved in the title reaction, for example, H, H_2, CHS, CH_2S, CH_3S, CH_3SH, and so on. Under the current computational conditions, the calculated geometrical parameters of the gas-phase CH_3SH, d_{S-H} = 1.336(1.340) Å, d_{C-S} = 1.816(1.819) Å, d_{C-H} = 1.078(1.090) Å, and $\angle$(C−S−H) = 96.3 (96.5)°, are in excellent agreement with the experimental values given in the parentheses.[35] Furthermore, the energy of methanethiol dissociation into $CH_3S + H$ in the gas phase was calculated to be 3.82 eV, in good agreement with the experimental value (3.73 eV).[36]

Transition state (TS) searches were performed at the same theoretical level with the complete LST/QST method.[27−29,37] In this method, the linear synchronous transit (LST) maximization was performed, followed by an energy minimization in directions conjugating to the reaction pathway to obtain an approximated TS. The approximated TS was used to perform quadratic synchronous transit (QST) maximization, and then another conjugated gradient minimization was performed. The cycle was repeated until a stationary point was located. The convergence criterion for the TS searches was set to 0.01 hartree/Å for the root-mean-square of atomic forces.

The adsorption energies reported herein were calculated using the equation:

$$E_{ads} = E_{adsorbate} + E_M - E_{adsorbate/M}$$

where E_{ads} is the adsorption energy of the adsorbate on the metal surface, $E_{adsorbate/M}$ is the energy of the adsorbate/M adsorption system, and $E_{adsorbate}$ and E_M are the energies of the free adsorbate and the clean slab, respectively. By this definition, stable adsorption will have a positive adsorption energy. At the present theoretical level, the adsorption energies for S at fcc and hcp sites on Pt(111) were calculated to be 4.69 and 4.50 eV, compared to the respective values of 4.54 and 4.26 eV calculated using the GGA-PBE functional and designed nonlocal (DNL) pseudopotentials implemented in the CPMD code,[38] and 4.94 and 4.75 eV calculated using the GGA-PBE96 functional and all-electron full-potential linearized augmented plane-wave (FLAPW) potential in the WIEN2k code.[39]

Test calculations were also performed using a four-layer $p(3 \times 3)$ unit cell, in which a Monkhorst−Pack mesh of $(3 \times 3 \times 1)$ k-points was employed and the other settings were the same as those for the

(26) Gate, B. C. *Catalytic Chemistry*; Wiley: New York, 1992.
(27) Delley, B. *J. Chem. Phys.* **1990**, *92*, 508.
(28) Delley, B. *J. Chem. Phys.* **1996**, *100*, 6107.
(29) Delley, B. *J. Chem. Phys.* **2000**, *113*, 7756.
(30) Perdew, J. P.; Wang, Y. *Phys. Rev. B* **1986**, *33*, 8800.
(31) Perdew, J. P.; Wang, Y. *Phys. Rev. B* **1992**, *45*, 13244.
(32) Popa, C.; Offrmans, W. K.; Santen, R. A. V.; Jansen, A. P. J. *Phys. Rev. B* **2006**, *74*, 155428.
(33) Monkhorst, H. J.; Pack, J. D. *Phys. Rev. B* **1976**, *13*, 5188.
(34) Hayek, K.; Glassl, H.; Gutmann, A.; Leonhard, H.; Prutton, M.; Tear, S. P.; Welton-Cook, M. R. *Surf. Sci.* **1985**, *152*, 419.
(35) Lide, D. R. *CRC Handbook of Chemistry and Physics*, 81st ed.; CRC Press: Boca Raton, FL, 2001.
(36) Nicovic, J. M.; Kreutter, K. D.; Van Dijk, C. A.; Wine, P. H. *J. Phys. Chem.* **1992**, *96*, 2518.
(37) Halgren, T. A.; Lipscomb, W. N. *Chem. Phys. Lett.* **1977**, *49*, 225.
(38) Lin, X.; Ramer, N. J.; Rappe, A. M.; Hass, K. C.; Schneider, W. F.; Trout, B. L. *J. Phys. Chem. B* **2001**, *105*, 7739.
(39) Yang, Z.; Wu, R.; Rodriguez, J. A. *Phys. Rev. B: Condens. Matter* **2002**, *65*, 155409.

Table 1. Adsorption Sites, Adsorption Energies (eV), and Structural Parameters (Å and deg) for Intermediates Involved in Methanthiol Decomposition on Pt(111)

species	sites	configuration[a]	E_{ads}[b]	$d_{C/H-Pt}$	d_{S-Pt}	d_{C-S}	angles[c]
CH_3SH*	top	η^1-S	1.01 (1.05)		2.329	1.818	64
CH_2SH*	bridge	$\eta^1-C-\eta^1-S$	2.56 (2.71)	2.059	2.352	1.845	83
CH_3S*	bridge	η^2-S	2.59 (2.68)		2.331, 2.342	1.823	57
CH_2S*	fcc	$\eta^1-C-\eta^2-S$	2.75 (2.87)	2.045	2.342, 2.351	1.794	85
	hcp	$\eta^1-C-\eta^2-S$	2.70 (2.80)	2.052	2.349, 2.352	1.798	86
CHS*	fcc	$\eta^2-C-\eta^1-S$	3.52 (3.66)	2.075, 2.075	2.314	1.715	70
	hcp	$\eta^2-C-\eta^1-S$	3.50 (3.63)	2.076, 2.080	2.311	1.719	70
	bridge	$\eta^1-C-\eta^1-S$	3.30 (3.44)	1.922	2.317	1.650	79
	fcc[d]	$\eta^1-C-\eta^2-S$	3.27 (3.39)	1.922	2.409, 2.423	1.674	88
	hcp[d]	$\eta^1-C-\eta^2-S$	3.24 (3.35)	1.923	2.417, 2.418	1.680	87
SH*	bridge	η^2-S	2.71 (2.81)		2.365, 2.373		
	top	η^1-S	2.19 (2.28)		2.308		
CS*	fcc	η^3-C	3.03 (3.09)	2.052, 2.063, 2.063		1.612	0
	hcp	η^3-C	2.97 (3.02)	2.054, 2.061, 2.063		1.610	0
	bridge	η^2-C	2.80 (2.88)	1.982, 1.987		1.586	1
	bridge[d]	$\eta^1-C-\eta^1-S$	2.15 (2.21)	1.874	2.400	1.607	73
	top	η^1-C	2.48 (2.56)	1.815		1.546	0
C*	fcc	η^3-C	6.54 (6.65)	1.905, 1.909, 1.914			
	hcp	η^3-C	6.38 (6.48)	1.914, 1.916, 1.926			
S*	fcc	η^3-S	4.69 (4.74)		2.301, 2.304, 2.304		
	hcp	η^3-S	4.50 (4.55)		2.309, 2.309, 2.310		
CH*	fcc	η^3-C	6.38 (6.59)	2.013, 2.014, 2.022			
	hcp	η^3-C	6.26 (6.47)	2.010, 2.010, 2.022			
CH_2*	bridge	η^2-C	3.97 (4.19)	2.059, 2.063			
CH_3*	top	η^1-C	2.01 (2.20)	2.054			
H*	top	η^1-H	2.63 (2.85)	1.532			
	fcc	η^3-H	2.62 (2.75)	1.830, 1.838, 1.845			
	hcp	η^3-H	2.57 (2.69)	1.810, 1.855, 1.859			
	bridge	η^2-H	2.52 (2.74)	1.723, 1.726			

[a] $\eta^m-C-\eta^n-S$ denotes the adsorbate adsorbs via the C and S atoms with m and n surface metal atoms, respectively. [b] Parameters in parentheses are adsorption energies before zero-point energy corrections. [c] Values are angles between the surface normal and the C−S axis in the corresponding species. [d] Sites denote another possible stable adsorption structure, which is different from the normal configuration on the same site.

(2 × 2) unit cell. The adsorption energy of CH_3S on the larger slab was calculated to be 2.66 eV, compared to the value of 2.59 eV calculated with the smaller model. Also, the different models predicted small differences in the activation energies for the initial two steps involved in the methanethiol decomposition (see Table S1 in the Supporting Information). These facts indicate that the coverage effect is indeed not important.

For a reaction such as AB → A + B on a surface, the reaction energy was calculated on the basis of the following formula:

$$\Delta H = E_{(A+B)/M} - E_{AB/M}$$

where $E_{(A+B)/M}$ is the total energy for the coadsorbed A and B on surface M.

Vibrational frequencies were calculated for all initial (IS) and final (FS) states as well as the TSs from the Hessian matrix with the harmonic approximation, and the zero-point energy (ZPE) was calculated from the resulting frequencies.

Rate constant k for unimolecular decomposition of an adsorbed species on the surface was calculated using standard nonvariational harmonic transition state theory:[32,40]

$$k = \frac{k_B T}{h}\frac{Q_{TS}}{Q_{IS}} e^{-(E^{\circ}_{act}/k_B T)} = A\, e^{-(E^{\circ}_{act}/k_B T)}$$

where k_B is the Boltzmann constant and h is the Planck's constant; Q_{IS} and Q_{TS} are the partition functions at the IS and TS, respectively; E°_{act} is the ZPE-corrected energy barrier; T is the temperature; and A is the pre-exponential factor.

3. Results

This part is divided into two sections. In section 3.1, we give structures and energies for all stable adsorptions involved in the methanthiol decomposition. In section 3.2, we investigate the most likely reaction steps in order to gather a general view of the decomposition network, including the thermodynamical and kinetical data. For clarification, all energies reported herein are after ZPE corrections.

3.1. Structures and Energies of Adsorbed Intermediates. In this section, we present a detailed investigation of the important intermediates involved in methanthiol decomposition on Pt(111) at the surface coverage of 1/4 ML. Table 1 lists some important parameters for these intermediates, and the most stable adsorption configurations are shown in Figure 1.

Methanthiol (CH_3SH). Although the adsorption of methanthiol on Pt(111) has been extensively investigated,[8,14,21,41] exact knowledge for the adsorbed structure has not been established. It is generally believed that the adsorption leads to the rupture of the S−H bond in CH_3SH at low temperatures, giving coadsorbed hydrogen and thiolmethoxy. Our calculation shows that CH_3SH could stably stay through the sulfur atom at top site with the C−S axis tilted by 64° to the surface normal and the SH bond parallel to the surface (see Figure 1a). The adsorption energy is calculated to be 1.01 eV. Similar configuration was also obtained for methanthiol on Pd(111)[24] and Au(111).[25] However, the latter two surfaces account for relatively low adsorption energies for methanthiol, that is, 0.38 eV for Au(111)[25] and 0.80 eV for Pd(111).[24] The extremely weak adsorption on Au(111) accords well with the fact that Au is inert toward methanthiol.[42]

Thiohydroxymethyl (CH_2SH). To our knowledge, no experimental or theoretical structural information can be obtained for this adsorbate on Pt surfaces. The $\eta^1-C-\eta^1-S$ configuration

(40) Hill, T. L. *An Introduction to Statistical Thermodynamics*; Dover: New York, 1986.

(41) Lee, J. J.; Fisher, C. J.; Bittencourt, C.; Woodruff, D. P.; Chan, A. S. Y.; Jones, R. G. *Surf. Sci.* **2002**, *516*, 1.

(42) Rzeźnicka, I.; Lee, J.; Maksymovych, P.; Yates, J., Jr. *J. Phys. Chem. B* **2005**, *109*, 15992.

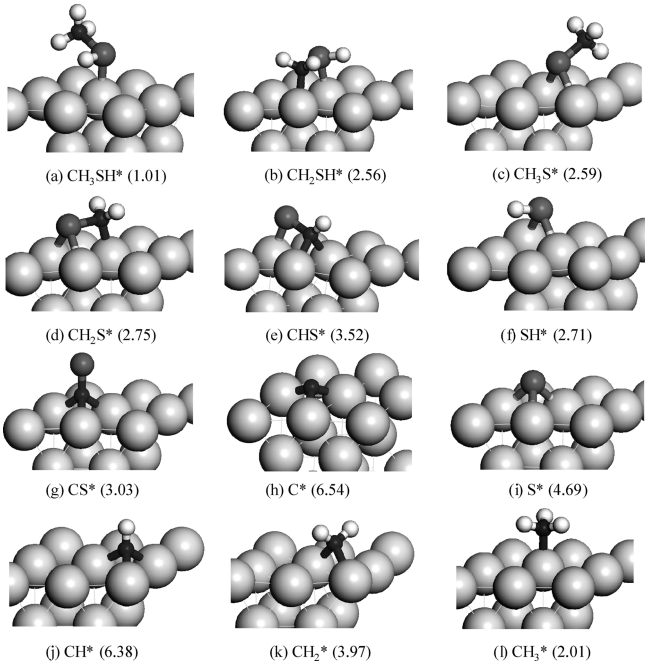

Figure 1. The most stable adsorption structures of intermediates involved in methanthiol decomposition on Pt(111). Value (in eV) in parentheses is the adsorption energy with ZPE correction for the corresponding species. The C, S, H, and Pt atoms are shown in the black, dark-gray, white, and light-gray colors, respectively.

with the adsorption energy of 2.56 eV is determined for CH_2SH on Pt(111) (see Figure 1b), in which both the C and S atoms sit at top sites through the sp^3 hybridized orbitals.

Thiolmethoxy (*CH_3S*). Thiolmethoxy is an important intermediate in methanthiol decomposition. It was reported that thiolmethoxy could adsorb stably at the top or bridge site on Pt(111).[8,14,18,41] In the present calculations, we find that, similar to the situation of Au(111),[22,25] the top adsorption is unstable, while the binding through the S atom over bridge site accounting for an adsorption energy of 2.59 eV is indeed located for thiolmethoxy (see Figure 1c). The S−Pt distances are 2.331 and 2.342 Å, and the C−S axis is calculated to be tilted 33° from the surface plane, compared to the experimental value of 45 ± 10°;[8] the vertical distance between S and the Pt surface is 1.831 Å, in good agreement with the experimental result of 1.9 ± 0.07 Å.[41]

Thioformaldehyde (*CH_2S*). Consistent with the experimental findings,[14] thioformaldehyde could be adsorbed in the η^1−C−η^2−S configuration over fcc and hcp on Pt(111) (see Table 1 and Figure 1d). The calculated bond lengths are 2.342−2.351 Å for S−Pt and 2.045 Å for C−Pt. The sulfur atom is found to be closer to the surface than the carbon atom, with the C−S axis tilted by ca. 5°, compared to the experimental value of 20° ± 10° estimated using HREELS and NEXAFS methods.[8] The almost identical adsorption energies (2.75 (fcc) and 2.70 (hcp) eV) suggest the comparable preference of these configurations.

Thioformyl (*CHS*). Further dehydrogenation of thioformaldehyde accounts for thioformyl. As listed in Table 1, thioformyl has five possible stable adsorption configurations on Pt(111), that is, fcc,hcp-η^2−C−η^1−S, fcc,hcp-η^1−C−η^2−S, and bridge-η^1−C−η^1−S, with the adsorption energies in the range of 3.24−3.52 eV. The presence of the bridge-η^1−C−η^1−S configuration makes the conversions between fcc,hcp-η^2−C−η^1−S and fcc,hcp-η^1−C−η^2−S (see Figure 1e) become easy.

Sulfydryl (*SH*). Sulfydryl is a short-lived intermediate that is difficult to observe experimentally, but it emerges as a critical intermediate for its relevance to catalytic reforming and HDS processes.[1,2,43] Our calculations reveal that SH stably binds at bridge (see Figure 1f) and top sites with the adsorption energies of 2.71 and 2.19 eV, respectively, compared to the previous DFT results (3.00 and 2.39 eV).[43] At both sites, the S−H bond lies more or less flat over the surface via the S end, in line with the HREELS finding.[44]

Carbon Monosulfide and Hydrogen (*CS and H*). Our calculation indicates that CS tends to bind upright at hollow sites through the carbon end with chemisorption energies of 3.03 (fcc) and 2.97 (hcp) eV (see Figure 1g). The adsorption of hydrogen over Pt(111) has been extensively investigated.[45−47] At the present theoretical level, the binding energies of H at the top, fcc, hcp, and bridge sites are very close in value (see Table 1), in agreement with the DFT study by Papoian et al.,[45] suggesting that atomic H could diffuse over the surface readily. The significant mobility of adsorbed H is expected to favor the dehydrogenation process.

Carbon and Sulfur (*C and S*). As is well-known, both coke formation and sulfur poisoning are severe problems that should be overcome in catalytic reforming applications. Although a significant number of studies have been performed on these topics,[39,48] it is necessary to understand the formation and distribution of carbon, sulfur, and relevant intermediates at the atomic scale. Similar to the situation of Ni(111),[49] C is stably adsorbed at the hollow sites on Pt(111) (d_{C-Pt} = 1.910 Å) with binding energies of 6.54 (fcc) and 6.38 (hcp) eV (see Figure 1h), in agreement with the previous theoretical result (6.41 eV for fcc).[48] For the atomic sulfur, we found fcc and hcp are the stable sites with adsorption energies of 4.69 and 4.50 eV (see Figure 1i), respectively, lower than the results of the previous DFT study (4.94 (fcc) and 4.75 (hcp) eV),[39] due perhaps to the fundamental difference between the pseudopotential approach used in our calculations and the FLAPW approach in ref 39. Top and bridge sites are unstable for both S and C, which would move to the fcc site during optimization, indicating the low mobility of S and C on Pt(111).

Methyne (*CH*). CH prefers the hollow sites via the C end in an upright manner on Pt(111) (see Figure 1j). For both the fcc and hcp adsorptions, the C atom is about 1.12 Å above the metal surface, and the C−Pt bonds are 2.010−2.022 Å long. These configurations account for almost equivalent binding energies (~6.3 eV), in agreement with the previous DFT finding (6.36 eV).[48]

Methylene (*CH_2*). Methylene is stably adsorbed at the bridge site on Pt(111), favoring a tetrahedral configuration, in which the H−C−H angle is 113° and the two C−Pt bonds are 2.059 and 2.063 Å long (see Figure 1k). The calculated adsorption energy is 3.97 eV, in agreement with the previous DFT value (4.13 eV).[48]

Methyl (*CH_3*). Methyl is only upright adsorbed at top site through the C atom, the C−Pt distance is 2.054 Å, and the H−C−H angle is 111° (see Figure 1l). This configuration accounts for an adsorption energy of 2.01 eV, in line with the previous DFT result (2.16 eV).[48]

3.2. Decomposition of Adsorbed Intermediates. In this section, we present the decomposition of the intermediates relevant

(43) Michaelides, A.; Hu, P. *J. Chem. Phys.* **2001**, *115*, 8570.
(44) Koestner, R. J.; Salmeron, M.; Kolin, E. B.; Gland, J. L. *Surf. Sci.* **1986**, *172*, 668.
(45) Papoian, G.; Nørskov, J. K.; Hoffmann, R. *J. Am. Chem. Soc.* **2000**, *122*, 4129.
(46) Greeley, J.; Mavrikakis, M. *J. Am. Chem. Soc.* **2002**, *124*, 7193.
(47) Greeley, J.; Mavrikakis, M. *J. Am. Chem. Soc.* **2004**, *126*, 3910.
(48) Jacob, T.; Goddard, W. A. *J. Phys. Chem. B* **2005**, *109*, 297.
(49) Watwe, R. M.; Bengaard, H. S.; Rostrup-Nielsen, J. R.; Dumesic, J. A.; Norskov, J. K. *J. Catal.* **2000**, *189*, 16.

Table 2. Calculated Energy Barriers E_a (eV), Reaction Energies ΔH (eV), Pre-Exponential Factor ν (s^{-1}), and Rate Constants k (s^{-1}) for the Elementary Reactions Involved in Methanthiol Decomposition on Pt(111)[a]

reaction	E_a	ΔH[b]	ν[c]	k[c]
$CH_3SH^* \rightarrow CH_3S^* + H^*$	0.18 (0.26)	−0.46 (−0.45)	1.23×10^{14}	1.28×10^{11}
$CH_3SH^* \rightarrow CH_2SH^* + H^*$	1.06 (1.27)	−0.06 (0.05)	3.02×10^{15}	5.46×10^{-3}
$CH_3SH^* \rightarrow CH_3^* + SH^*$	1.94 (2.06)	−0.2 (−0.17)	5.52×10^{14}	1.52×10^{-18}
$CH_3S^* \rightarrow CH_2S^* + H^*$	0.96 (1.10)	−0.17 (−0.12)	3.59×10^{14}	2.43×10^{-2}
$CH_3S^* \rightarrow CH_3^* + S^*$	1.03 (1.13)	−0.43 (−0.41)	1.80×10^{14}	7.82×10^{-4}
$CH_2S^* \rightarrow CHS^* + H^*$	1.35 (2.03)	0.92 (0.86)	4.15×10^{16}	9.26×10^{-7}
$CH_2S^* \rightarrow CH_2^* + S^*$	1.45 (1.53)	0.47 (0.49)	2.24×10^{14}	8.77×10^{-11}
$CHS^* \rightarrow CS^* + H^*$	1.42 (1.61)	0.35 (0.45)	1.10×10^{16}	1.38×10^{-8}
$CHS^* \rightarrow CH^* + S^*$	0.66 (0.71)	−0.34 (−0.37)	3.20×10^{13}	3.07×10^{2}
$CH^* \rightarrow C^* + H^*$	1.56 (1.70)	0.99 (1.16)	2.03×10^{17}	5.61×10^{-15}
$CS^* \rightarrow C^* + S^*$	0.88 (0.89)	0.40 (0.37)	2.03×10^{12}	3.56×10^{-3}
$SH^* \rightarrow S^* + H^*$	0.15 (0.23)	−0.56 (−0.59)	3.13×10^{11}	9.81×10^{13}

[a] Values in parentheses are energies before zero-point-energy corrections. [b] Values are obtained by subtracting the energies of the IS from those of the FS. [c] Values are calculated at 300 K.

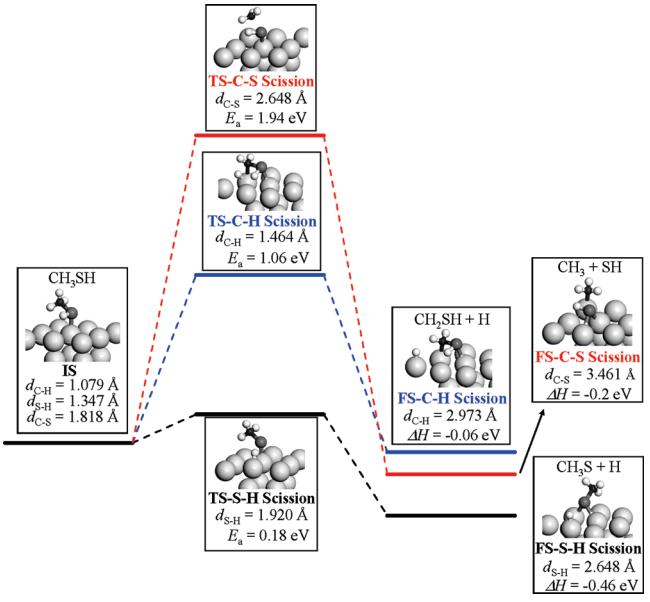

Figure 2. Reaction pathways of CH_3SH. IS, initial state; TS, transition state; FS, final state. E_a denotes energy barrier for the corresponding step, and ΔH represents the relevant reaction energy.

to the main decomposition pathways of methanthiol on Pt(111), via S−H, C−H, and C−S bond scission. For simplicity, we choose the adsorption of the involved intermediate at the most stable site as the IS, and the corresponding FS is taken to be the coadsorption of the product species at their most stable sites. Note that, although CH_2SH is not included in the most favorable pathway, we still carefully study its sequential decomposition via the possible (S−H, C−H, and C−S) bond scissions in order to give a complete map of the CH_3SH decomposition; detailed information is presented in the Supporting Information. The thermochemical and kinetical parameters of all the elementary steps considered are summarized in Table 2.

3.2.1. Methanthiol Decomposition. It can be envisioned that methanthiol decomposition may involve S−H, C−H, and/or C−S bond scission. The decomposition PES together with the schematic structures involved is shown in Figure 2.

S−H Bond Scission. The S−H path yields thiolmethoxy and atomic H, with the activation barrier of only 0.18 eV and the reaction energy of −0.46 eV. As shown in Figure 2, a slight rotation of the adsorbed methanthiol results in the activation of the S−H bond. In the TS of this step, the CH_3S fragment remains its top site through the S atom, and the atomic H sits at adjacent top site; the corresponding bond lengths (d_{S-H} = 1.920 Å; d_{Pt-H} = 1.579 Å) suggest that the S−H bond has been ruptured and the Pt−H bond has been formed. After the TS, the atomic H remains the top site, and the CH_3S fragment moves to its most stable (bridge) site, forming the FS.

C−H Bond Scission. C−H bond scission in CH_3SH produces thiohydroxymethyl and atomic H. This process results from the incline of the C−S axis such that Pt could insert into one of the C−H bonds. In the TS, the CH_2SH entity is almost at its stable site; the atomic H sits at an off-top site sharing a Pt atom with C; and the C−H* and C−Pt distances are 1.464 and 2.289 Å, respectively. After the TS, CH_2SH stays still at the bridge site with the C−Pt distance further shortened (2.067 Å), and the atomic H moves to adjacent top site because of strong repulsion of CH_2SH. This step accounts for an activation barrier of 1.06 eV and a reaction energy of −0.06 eV.

C−S Bond Scission. The C−S path is facilitated by the stretching vibration of CH_3−SH. At the TS, SH still binds at the top site via the S end, and the CH_3 group is isolated from both the SH moiety and the surface. After the TS, the SH moves toward the neighboring bridge site and CH_3 moves down to top site of the surface, forming the FS. This step is exothermic by 0.2 eV, but it is hindered by a very high barrier (1.94 eV).

3.2.2. Thiomethoxy Decomposition. It can be envisioned that decomposition of thiomethoxy may involve C−H and C−S bond scission. Figure 3 gives the decomposition PES as well as the schematic structures involved.

C−H Bond Scission. The C−H path of CH_3S yields CH_2S and atomic H. As shown in Figure 3, this process results from the incline of the C−S axis so that one of the methyl H atoms could migrate to adjacent top site. When the relevant TS is located, the C−H bond is ruptured and the Pt−H bond is formed mirrored by the corresponding bond distances (1.538 and 1.597 Å). Subsequently, arrangement of the fragment species to their most stable sites accounts for the FS. The activation barrier of this step is 0.96 eV, and the reaction energy is −0.17 eV.

C−S Bond Scission. Similar to the situation of methanthiol, the C−S path of CH_3S is activated with the help of the C−S bond stretching vibration, producing S and CH_3. In the TS, S atom sits nearly at the fcc site and the CH_3 group is isolated from both the S atom and the surface. Following the TS, the S atom remains the fcc site, while CH_3 group moves down to the top site, giving the FS. This step is hindered by a barrier of 1.03 eV, and it is exothermic by 0.43 eV.

3.2.3. Thioformaldehyde Decomposition. Bond cleavage of thioformaldehyde contains also two possibilities, that is, C−H and C−S bond scission. The decomposition PES and schematic structures involved are presented in Figure 4.

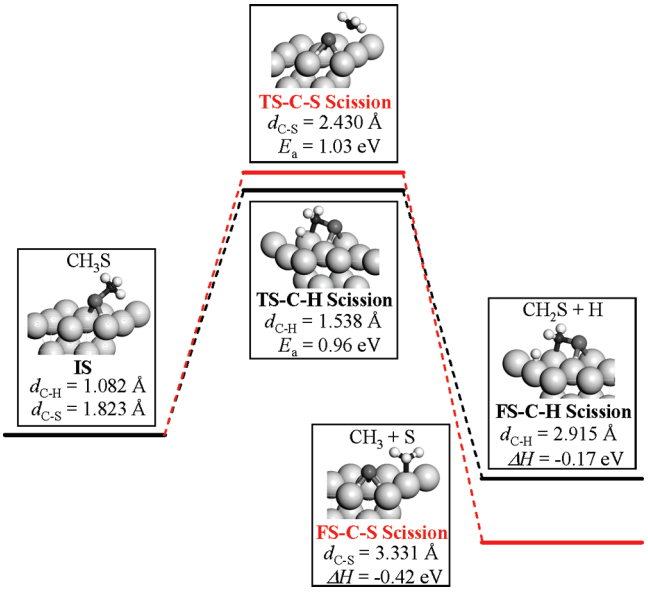

Figure 3. Reaction pathways of CH_3S. Parameters follow the same notation as in Figure 2.

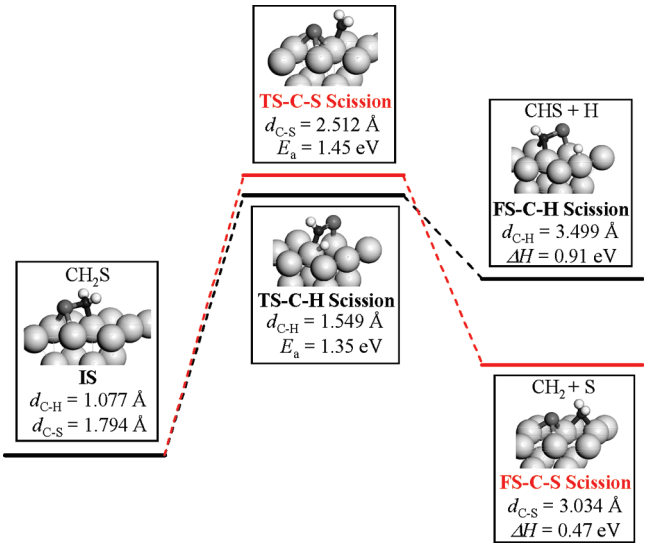

Figure 4. Reaction pathways of CH_2S. Parameters follow the same notation as in Figure 2.

C−H Bond Scission. In this path, intrarotation of the CH_2 group along the C−S axis brings one of the methylene H close to the surface so that the C−H bond is activated, giving CHS and atomic H as the product, endothermic by 0.92 eV. In the TS, the H* and C atoms share one surface Pt atom with the C−H and Pt−H distances being 1.549 and 1.883 Å, respectively. This TS configuration affords an energy barrier of 1.35 eV. After the TS, the CHS entity remains in the η^2−C−η^1−S configuration at the hcp site, and the atomic H moves to an adjacent top site because of strong repulsion of CHS.

C−S Bond Scission. This path gives CH_2 and atomic S due also to the C−S stretching vibration. In this case, the atomic S move to the neighboring fcc site and CH_2 group toward the opposite direction along C−S axis. The C−S distance elongates from 1.794 Å at the IS to 2.512 Å at the TS. In the FS, the CH_2 group binds at the bridge site and the atomic S at the fcc site. The barrier of this step is 1.45 eV, and the reaction energy is 0.47 eV.

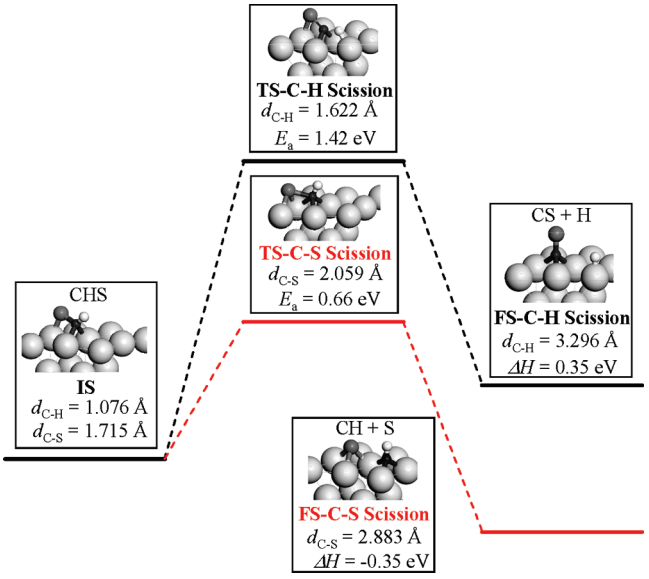

Figure 5. Reaction pathways of CHS. Parameters follow the same notation as in Figure 2.

3.2.4. Thioformyl Decomposition. Thioformyl dissociation also involves C−H and/or C−S bond scission. The decomposition PES as well as the schematic structures involved are shown in Figure 5.

C−H Bond Scission. The C−H path of CHS yields CS and atomic H. A swag vibration of the adsorbed CHS makes the H atom approach the surface and the S atom deviate from the surface. At the TS, the S−Pt distance elongates to 2.511 Å (2.314 Å in the IS), and the C−H bond length increases to 1.622 Å. In the FS, CS binds upright at the fcc site through the C atom, and the atomic H binds at top site. The calculated energy barrier of this step is 1.42 eV, and the reaction energy is 0.35 eV.

C−S Bond Scission. The C−S bond scission of CHS accounts for the formation of CH and atomic S. In the course of this reaction, the C−S bond breaks due to the C−S stretch vibration. The TS of this process has a geometry that S sits at bridge site, and the C atom at fcc site; the C−S distance elongates to 2.059 Å (1.715 Å at the IS). In the FS, the CH group binds at the fcc site with the atomic S at an adjacent fcc site. The barrier of this step is 0.66 eV, and the reaction energy is −0.34 eV.

3.2.5. Reaction of Methyne. Once methyne is produced, it may further decompose into atomic carbon and hydrogen or hydrogenate to methylene. Both possibilities are checked (see Figure S6 in the Supporting Information). The barrier for the hydrogenation process (CH + H → CH_2) is calculated to be 1.10 eV, and the barrier for the dehydrogenation process (CH → C + H) is 1.88 eV. These values are obviously higher than the previous DFT results calculated by Michaelides and Hu (0.72 and 1.53 eV), perhaps because of the fact that all substrate metal atoms were frozen.[50]

4. Discussion

In this section, we discuss some important points based on the calculated results.

4.1. General Structural Features for the Involved Intermediates. After getting the structures of $C_xH_ySH_z$ (x = 0, 1; y = 0−3; z = 0, 1) on Pt(111), we can give a general relationship between the preferred adsorption configuration and the bonding

(50) Michaelides, A.; Hu, P. *J. Am. Chem. Soc.* **2000**, *122*, 9866.

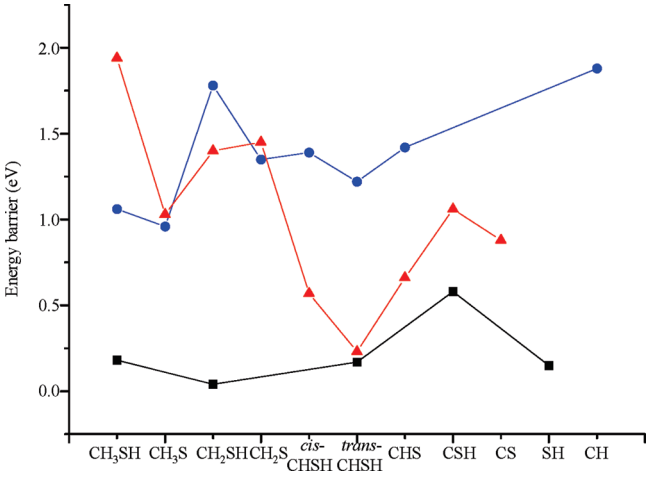

Figure 6. Curves of energy barriers for the S−H, C−H, and C−S bond scission of intermediates involved in the decomposition of methanthiol on Pt(111). The square, circle, and triangle symbols represent S−H, C−H, and C−S bond scissions, respectively.

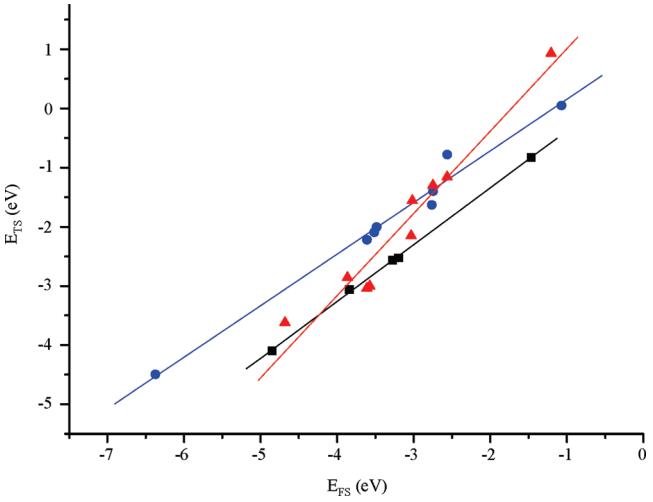

Figure 7. Plot of the TS energy against the FS energy for all the bond-scission reactions involved in methanthiol decomposition on Pt(111). The square, circle, and triangle symbols denote S−H, C−H, and C−S bond scissions, respectively.

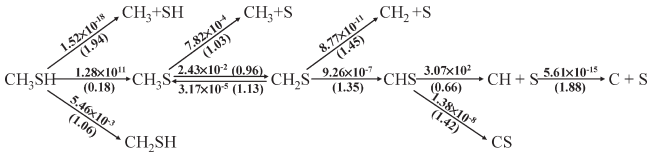

Figure 8. Decomposition network of methanthiol on Pt(111). The rate constant calculated at 300 K (s^{-1}) and activation barrier (in parentheses; eV) of each step are given.

ability of the involved C and S atoms by summarizing the structural features. It can be found that both C and S atoms in the most stable adsorption of the involved species tend to be sp^3 hybridized by bonding with H and/or surface metal atoms; that is, C is almost tetrahedral, and S has the tendency to bond to three atoms, with the lost atoms replaced by the metal atoms. For instance, η^1−S for CH_3SH; η^1−C for CH_3; η^2−S for CH_3S and SH; η^2−C for CH_2; η^3−S for S; η^3−C for CH; η^1−C−η^1−S for CH_2SH; η^2−C−η^1−S for *cis*-CHSH; and η^1−C−η^2−S for CH_2S. Note that this relation can also be applied to the C,S-containing species (CH_3SH and CH_3S) on other transition metal surfaces, such as Pd(111)[24] and Au(111),[25] but is different from their O-analogues adsorbed on VIII group metal (111) surfaces, that is, intermediates in the methanol and ethanol decomposition, in which C is really tetrahedral via sp^3 hybridization, but O is divalent.[46,51,52] This can be explained by the facts that the larger size of S results in the delocalization of S p orbitals and thus the atom can be oxidated more deeply.

4.2. Analysis of Energy Barriers for Bond Cleavage. Figure 6 gives energy barriers for the C−H, C−S, and S−H bond scission in intermediates involved in the CH_3SH decomposition. We can find that C−H bond scission always has higher energy barriers (> 1 eV), for example, ∼1 eV for CH_3SH and CH_3S, ∼1.3 eV for CH_2S, CHSH, and CHS, and ∼2.0 eV for CH_2SH and CH; energy barriers for S−H bond cleavage are indeed very low and change less (generally below 0.25 eV with the exception of 0.58 eV for CSH); for the C−S bond scission, the larger intermediates (CH_3SH, CH_3S, CH_2SH, and CH_2S) have the higher energy barriers that are comparable to those for the C−H path and barriers for the smaller intermediates (CHSH, CHS, CSH, and CS) are in-between the values of the C−H and S−H paths. These facts indicate that S−H bond scission would be preferred when available.

Furthermore, we make a comparison of the activation barrier and the heat of reaction (known as the Brønsted−Evans−Polanyi (BEP) behavior[53]) for each elementary step to determine whether there is a clear relationship in different bond cleavages. Following the framework suggested by Alcalà et al.,[54] the elementary reactions are written as exothermic steps, and the IS and FS are defined accordingly. The energy reference for each step is the clean slab plus gas-phase energy of the corresponding reactants. As shown in Figure 7, we can identify three distinct beelines for the S−H, C−H, and C−S bond scission reactions. This feature simply reflects that no single BEP relation can be established for all reactions on the same surface, whereas in each bond scission class a linear relationship holds for most reactions. Therefore, it is possible to estimate the transition state energies from the final state energies for the alkylthiol decomposition processes on Pt(111). The upper-left line is for the C−H path, in which $E_{TS} = 0.87E_{FS} + 1.03$ (eV), the corresponding square of the correlation coefficient is 0.99, and the standard error is 0.21 eV. The bottom-right line represents the S−H path, the linear regression equation is $E_{TS} = 0.96E_{FS} + 0.58$ (eV); the square of the correlation coefficient (nearly 1) as well as the standard error (0.04 eV) suggest that the BEP relation holds well. The line across the above two lines is for the C−S path, the linear regression equation is $E_{TS} = 1.39E_{FS} + 2.4$ (eV), and the square of the correlation coefficient and the standard error are 0.97 and 0.35 eV, respectively. Checking the structures involved in all the reactions, we found that, in line with the previous finding, the surface reaction following the BEP principle generally possesses a "late" TS,[54] and the TS structures do resemble the FS structures.

4.3. Reaction Pathways. In this section, we first elaborate the reactions of intermediates involved in the most likely pathway and then discuss the decomposition mechanism of CH_3SH on Pt(111). The reaction network for the methanthiol decomposition is given in Figure 8, in which the rate constants are calculated at the typical hydrogenation temperature (300 K).[12]

(51) Jiang, R. B.; Guo, W. Y.; Li, M.; Fu, D. L.; Shan, H. H. *J. Phys. Chem. C* **2009**, *113*, 4188.
(52) Li, M.; Guo, W. Y.; Jiang, R. B.; Zhao, L. M.; Shan, H. H. *Langmuir* **2010**, *26*, 1879.
(53) Liu, Z. P.; Hu, P. *J. Chem. Phys.* **2003**, *119*, 6282.
(54) Alcalà, R.; Mavrikakis, M; Dumesic, J. A. *J. Catal.* **2003**, *218*, 178.

For the surface CH_3SH, the S−H bond scission leading to CH_3S and atomic H is strongly favored because it has a barrier (0.18 eV) much lower than the barriers for the alternative C−H and C−S paths (1.06 and 1.94 eV) as well as the desorption energy of CH_3SH (1.01 eV), in agreement with the experimental evidence that CH_3S rather than CH_2SH or CH_3 was observed on Pt(111).[8,14] The lack of experimental evidence for stable CH_3SH existing on Pt(111) further demonstrates that at low coverage CH_3SH dissociates rapidly. In fact, CH_3SH is unstable on Pt(111) and Pd(111),[24] which would undergo spontaneously dissociative reaction of S−H bond cleavage due to the high exothermicity (0.46 and 0.79 eV) as well as the low energy barriers (0.18 and 0.10 eV). On Au(111),[25] however, decomposition of adsorbed CH_3SH is endothermic by 0.33 eV and prohibited by the relatively high energy barrier (0.52 eV); thus, it desorbs exclusively as experimentally confirmed.[42]

Intermediate CH_3S has two competitive decomposition paths via C−H and C−S bond scission with nearly identical activation barriers (0.96 vs 1.03 eV). However, rate constants for the CH_3S decomposition paths (see Table 2) indicate that the C−H path is more favorable under the UHV condition. Because of the low barrier for its formation and the relatively high barriers for its decomposition, CH_3S should be abundant on Pt(111), in good agreement with the experimental findings.[8,12,14,21] The barrier for CH_2S formation is much lower than the barriers for its decomposition, for either C−H or C−S path. Therefore, CH_2S can accumulate to a certain amount for observation, explaining the fact that CH_2S was also detected in experiments.[8,12,14,21] Furthermore, the C−H activation in CH_2S should be preferred because it has a lower energy barrier (1.35 vs 1.45 eV) and thus has a rate constant about 4 orders larger than that for the C−S activation (see Table 2). Species CHS is unstable on Pt(111) with a rather low barrier for its C−S bond scission (0.66 eV). Hence, once CHS is formed, it would decompose into CH and S readily. CH could either decompose to C and H or hydrogenate to adsorbed CH_2. It seems that CH hydrogenation is more favorable because of the relatively low barrier with respect to that for the alternative decomposition (1.10 vs 1.88 eV). However, the hydrogenation process is expected to be limited by the availability of surface atomic hydrogen, since the calculated barrier for the combinative desorption of hydrogen (H* + H* → H_2) is only 0.88 eV. As a result, CH should further decompose into C and H, in concert with the experimental result that H_2 was observed as the dominant product rather than hydrocarbons.[14,21]

Now, we turn to the decomposition mechanism of methanthiol. Figure 8 reveals that the rate constant of CH_3SH decomposition to CH_3S (1.28×10^{11} s^{-1}) is several orders larger than those of the other parallel and following paths, indicating the S−H bond scission of CH_3SH is indeed a rapid process. For the following reaction, we carry out a kinetic analysis to clarify the competition of C−S and C−H activation in CH_3S, in which the C−S bond scission occurs at different intermediates. We define the C−S bond scission occurring at CH_3S as path I, and the other as path II (reactions II.1−II.3), in which the C−S bond scission does not occur until the CHS intermediate is formed. In path II, we do not incorporate in the model the C−S path in CH_2S and the C−H path in CHS, because they have the rate constants at least 4 orders smaller than the alternative paths considered (see Figure 8). Based on the kinetic parameters given in Figure 8, the elementary steps involved in paths I and II are as follows:

$$CH_3S^* + * \xrightarrow{k_I} CH_3^* + S^* \quad (I)$$

$$CH_3S^* + * \underset{k_{-II1}}{\overset{k_{II1}}{\rightleftharpoons}} CH_2S^* + H^* \quad (II.1)$$

$$CH_2S^* + * \xrightarrow{k_{II2}} CHS^* + H^* \quad (II.2)$$

$$CHS^* + * \xrightarrow{k_{II3}} CH^* + S^* \quad (II.3)$$

Here "*" represents a surface site. The total reaction rate of path I, $r(I)$, can be expressed as

$$r(I) = k_I \theta_{CH_3S} \theta_*$$

where θ_X represents the surface coverage of adsorbate X. In path II, rate constants for the forward and reverse reactions of step II1 (k_{II1} and k_{-II1}) are obviously both larger than that of step II2 (k_{II2}), leading to a swift equilibrium of step II1; so $k_{II1}\theta_{CH_3S}\theta_* = k_{-II1}\theta_{CH_2S}\theta_H$ and thus $\theta_{CH_2S} = K_{II1}[(\theta_{CH_3S}\theta_*)/\theta_H]$, where K_{II1} is the relevant equilibrium constant obtained using $K_{II1} = k_{II1}/k_{-II1}$. For the following reactions in path II, step II.2 is obviously the rate limiting step because of the much lower rate constant (k_{II2}) compared to that of step II.3 (k_{II3}) (see Figure 8); thus, the total reaction rate of path II, $r(II)$, can be represented as

$$r(II) = k_{II2}\theta_{CH_2S}\theta_*$$

Combined with the formula of θ_{CH_2S}, we obtain

$$r(II) = k_{II2}\theta_{CH_2S}\theta_* = k_{II2}K_{II1}\frac{\theta_{CH_3S}\theta_*^2}{\theta_H}$$

Thus, at the experimental temperature (300 K),[12]

$$\frac{r(I)}{r(II)} = \frac{k_I\theta_H}{k_{II2}K_{II1}\theta_*} = 1.1\frac{\theta_H}{\theta_*}$$

It is clear that, under the hydrogenation condition ($\theta_H > \theta_*$), $r(I) > r(II)$ and thus the C−S bond scission of CH_3SH on Pt(111) mainly occurs at CH_3S (path I), explaining the experimental results that, in the presence of hydrogen, CH_4 is the primary product for the decomposition of methanethiol at around 300 K.[12]

In the absence of hydrogen ($\theta_H < \theta_*$), $r(I) < r(II)$ and thus the C−S bond scission mainly occurs at CHS (path II), and only a small amount of C−S bond scission takes place at CH_3S. Furthermore, because CH_2S decomposition into CHS needs to overcome an energy barrier higher than that for its formation, it can be predicted that, in the absence of H_2, most of C−S bond scission would occur at relatively high temperatures. This is in good agreement with the experimental results that a large fraction of C−S bond scission does not occur until 450 K in the UHV condition.[12] Thus, the whole decomposition pathway can be written as $CH_3SH \rightarrow CH_3S \rightarrow CH_2S \rightarrow CHS \rightarrow CH + S \rightarrow C + S$, obviously different from the decomposition path of $CH_3SH \rightarrow CH_3S \rightarrow CH_2S \rightarrow CHS \rightarrow CS \rightarrow C + S$ proposed on the basis of the previous experimental works.[14,18,21,41] The C−S bond scission occurring at intermediate CS proposed in experiments was mainly based on the observations that at low coverage surface Pt exhibits a catalytic effect on CH_xS dehydrogenation, which leads to the formation of intermediates, for example, CH_3S and CH_2S; thus, sequential dehydrogenation was presumed and C−S bond

scission was deduced to occur until all the C−H bonds have broken.

5. Conclusions

First principle periodic DFT calculations have been used to study the thermochemistry and kinetics of methanthiol decomposition on Pt(111). The decomposition network has been mapped out. The most stable adsorption of the involved species tends to form the sp^3 hybridized configuration of both C and S atoms; that is, C is almost tetrahedral and S has the tendency to bond to three atoms with the lost H atoms being replaced by the metal atoms. CH_3SH adsorbs strongly on the top site through the S atom. CH_3S binds stably at the bridge site. Both CH_2S and CHS prefer threefold hollow sites. Adsorbed CH_3SH on Pt(111) undergoes spontaneous S−H bond cleavage. Intermediates CH_3S and CH_2S in the pathway have relatively low decomposition rate constants compared with the rate constants for their formation, explaining the fact that lifetimes of CH_3S and CH_2S species on Pt(111) are long enough for direct experimental observations. Through the kinetic analysis of the elementary steps, the most likely decomposition pathway of CH_3SH under the UHV condition is identified as $CH_3SH \rightarrow CH_3S \rightarrow CH_2S \rightarrow CHS \rightarrow CH + S \rightarrow C + S$, in which the C−S bond scission mainly occurs at CHS species; under the hydrogenation condition, the C−S bond scission mainly occurs at CH_3S species. The Brønsted−Evans−Polanyi relation holds for each of S−H, C−H, and C−S bond scission reactions.

Acknowledgment. This work was supported by the Program for Changjiang Scholars and Innovative Research Team in University (IRT0759) of MOE, PRC, NSFC (20476061 and 10979077), State Key Basic Research Program of China (2006CB202505), CNPC Science & Technology Innovation Foundation (2009D-5006-04-07), and Independent Innovation Program of China University of Petroleum (09CX05002A).

Supporting Information Available: Calculated results for the initial two steps of methanethiol decomposition at 1/9 ML and information of CH_2SH decomposition and CH reactions at 1/4 ML. This material is available free of charge via the Internet at http://pubs.acs.org.